Arch. Metall. Mater. **65** (2020), 3, 993-996

DOI: 10.24425/amm.2020.133204

NU SI A EOM[1], MUHAMMAD ANEEQ HAQ[1], JIMIN LEE[2], KYOUNG-MOOK LIM[1],
TAEK SOO KIM[3], YONG-HO CHOA[2], BUM SUNG KIM[1*]

CONTROL OF Nd-Fe-B MORPHOLOGY AS FUNCTION OF THE PVP CONCENTRATION USING ELECTROSPINNING PROCESS

In this study, we demonstrate a facile and cost-effective way to synthesize Nd-Fe-B of various shapes such as powders, rods and fibers using electrospinning, heat-treatment and washing procedures. Initially Nd-Fe-B fibers were fabricated using electrospinning. The as-spun Nd-Fe-B fibers had diameters ranging 489 to 630 nm depending on the PVP concentration in reaction solutions. The different morphologies of the $Nd_2Fe_{14}B$ magnetic materials were related to the difference in thickness of the as-spun fibers. The relationships between the as-spun fiber thickness, the final morphology, and magnetic properties were briefly elucidated. The intrinsic coercivity of $Nd_2Fe_{14}B$ changed with the change in morphology from powder (3908 Oe) to fiber (4622 Oe). This work demonstrates the effect of the Nd-Fe-B magnetic properties with morphology and can be extended to the experimental design of other magnetic materials.

Keywords: $Nd_2Fe_{14}B$, 1-D magnet fiber, Electrospinning, Magnet properties, Morphology

1. Introduction

The development of permanent magnet materials such as neodymium-iron-boron (Nd-Fe-B), samarium-cobalt (Sm-Co), and samarium-iron-nitride (Sm-Fe-N) has led to the rise of innovations such as permanent magnet motors, hybrid electric vehicles, and electric generators in an effort to conserve energy [1-3]. Among the various magnetic materials, the Nd-Fe-B permanent magnets are the most prevalent due to their tetragonal crystal structure having uniaxial magneto-crystalline anisotropy ($H_A \approx 7$ T) [4]. Further improvement in the magnetic properties of the NdFeB magnets has been reported by partially replacing Nd with other rare earth (RE) elements such as dysprosium (Dy) and terbium (Tb) [5]. However, this approach leads to an increase in production cost due to high costs of RE elements. Another method to enhance magnetic properties of Nd-Fe-B materials is the fabrication of the permanent magnet with a different morphology, such as a 1-dimensional morphology. The 1-dimensional structures such as tubes, rods, and fibers can have high shape anisotropy which acts to align the magnetization along the longest direction [6]. The high aspect ratio of a 1-dimensional structure can increase coercivity because of its shape anisotropy [7].

Generally, powder metallurgy [8] and rapid quenching [9] are conventional top-down processes used to fabricate the Nd-Fe-B permanent magnet. However, it is difficult to control the morphology of the magnet with these methods, and a novel approach which can produce a different Nd-Fe-B morphology is required. The electrospinning method is a bottom-up process which can easily produce the 1-dimensional structured materials at the submicron scale [10]. It can control the thickness of the magnetic fibers by adjusting the quantities of each ingredient, typically polymer [11], which is a material that affects the thickness of fibers by controlling the viscosity of the precursor solution. In addition, the powder particles can be fabricated from fibers through washing process after electrospinning and heat treatment [12]. This process makes it possible to compare the characteristics of the Nd-Fe-B with various morphologies, including 1-dimensinal morphologies such as rod and fibers.

In this study, we have compared the magnetic properties of different morphologies of Nd-Fe-B materials. The final morphology was controlled by a combination of electrospinning, heat

[1] KOREAN INSTITUTE FOR RARE METALS, KOREA INSTITUTE OF INDUSTRIAL TECHNOLOGY, 156, GAETBEOL-RO, YEONSU-GU, INCHEON, 21999, REPUBLIC OF KOREA
[2] HANYANG UNIVERSITY, DEPARTMENT OF MATERIALS SCIENCE AND CHEMICAL ENGINEERING, 55, HANYANGDAEHAK-RO, SANGNOK-GU, ANSAN-SI, GYEONGGI-DO 15588, REPUBLIC OF KOREA
[3] RESEARCH INSTITUTE OF ADVANCED MANUFACTURING TECHNOLOGY, KOREA INSTITUTE OF INDUSTRIAL TECHNOLOGY, 156, GAETBEOL-RO, YEONSU-GU, INCHEON, 21999, REPUBLIC OF KOREA

* Corresponding author: bskim15@kitech.re.kr

treatment and washing process. In order to control morphology of Nd-Fe-B materials, the thicknesses of as-spun Nd-Fe-B fibers were adjusted by the varying the PVP concentration. The magnetic properties of the Nd-Fe-B materials synthesized with various morphologies are discussed using the M-H hysteresis curve and the dependence of the morphology changes from 0-dimension to 1-dimension.

2. Experimental

Neodymium nitrate hexahydrate ($Nd(NO_3)_3 \cdot 6H_2O$, 99.9%, Sigma-Aldrich Inc., Korea), iron nitrate nonahydrate ($Fe(NO_3)_3 \cdot 9H_2O$, 98%, Junsei Inc., Korea), boric acid ($B(OH)_3$, 99.5%, Sigma-Aldrich Inc., Korea), and polyvinylpyrrolidone (PVP, $M_w \approx 1{,}300{,}000$, Sigma-Aldrich Inc., Korea) were used to prepare the precursor solution for electrospinning. Calcium (Ca, 99.5%, Alfa Aesar Co., Inc., England) was used as a reductant.

In order to match the stoichiometric ratio of the electrospinning precursor, the composition was adjusted to the ratio of 2.2:14:1.1 (Nd:Fe:B). While maintaining the amounts of Nd, Fe, and B, the thickness of the fiber was adjusted by changing only the concentration of PVP (3.15, 3.75, 4.35 wt%) to control the morphology of the electrospun fibers. The viscosity of the precursor solutions as a function of PVP was measured by a viscometer (DL2TLV, Brookfield Engineering Laboratories, Inc., USA) at room temperature. The electrospinning step for fiber fabrication was applied using Nanospider equipment (NSLAB, Elmarco Inc., Republic of Czech). The synthesized precursor was loaded in a Nanospider carrier whose moving speed was 300 mm/s and applied voltage was 50 kV. Organic elements of the fabricated fibers were removed by calcination at 900°C under air condition, and oxide fibers were mixed with the calcium as a reductant and reduced at 700°C under argon condition. After reduction, the oxide becomes $Nd_2Fe_{14}B$, an intermetallic compound, through in-situ reduction diffusion. Calcium oxide, a byproduct of the reduction reaction, was removed by washing. The washed samples were dried in an oven at 80°C.

The phase changes of each heat treatment step were analyzed by X-ray diffraction (XRD, Bruker Co., USA) by using a Cu Kα radiation. Morphology and diameter of the fibers were analyzed by a field emission scanning electron microscope (FE-SEM, JSM-7100F, JEOL Ltd., Japan). The M-H hysteresis curve that shows magnetic properties of magnetic fibers after washing were obtained at room temperature by a vibrating sample magnetometer (VSM, VersaLab VSM, Quantum Design Co., USA) under the maximum field of 3 T.

3. Results and discussion

Fig. 1 shows the X-ray diffraction patterns with fabricated magnetic materials of 3.15 wt% PVP concentration measured for each step, that is, electrospinning, calcination, reduction, and washing. All phase data were obtained from the crystallography open database (COD). The phases are $FeNdO_3$ (COD No. 2003124), Fe_2O_3 (COD No. 9014880), $NdBO_3$ (COD No. 7209470), CaO (COD No. 1000044), and $Nd_2Fe_{14}B$ (COD No. 1511143). Fig. 1(a) shows as-spun fibers, which have no specific crystallized peaks. After the heat treatment, as-spun fibers were converted into metal oxides fibers. Fig. 1(b) shows the metallic oxide, which has a crystal structure through nucleation and growth, during the calcination step [13]. Two dominant peaks, Fe_2O_3 and $NdFeO_3$, were observed. Below are the oxidation reaction equations that can explain how nitride fibers formed into oxide fibers.

$$4Nd(NO_3)_3 + 3O_2(g) \rightarrow 2Nd_2O_3 + 12NO_3(g) \quad (1\text{-}1)$$

$$3Fe(NO_3)_3 + 2O_2(g) \rightarrow Fe_3O_4 + 9NO_3(g) \quad (1\text{-}2)$$

$$2Nd_2O_3 + 4Fe_3O_4 + O_2(g) \rightarrow 4FeNdO_3 + 4Fe_2O_3 \quad (1\text{-}3)$$

These oxides became $Nd_2Fe_{14}B$ through the continuous reduction-diffusion process. Fig. 1(c) shows that there are two peaks of CaO and $Nd_2Fe_{14}B$ with no oxide peak, indicating that all the oxides react during the reduction process; the peak intensity of XRD shows that that of CaO was much higher than that of $Nd_2Fe_{14}B$. In the reduction-diffusion process, metallic oxides were reduced by calcium, which remained in the material in the form of CaO. Below are reduction reaction equations (3) between oxide fibers and calcium [14,15].

$$NdFeO_3 + Fe_2O_3 + FeB + \\ + Ca \rightarrow Nd_2Fe_{14}B + CaO \quad (3)\ [15]$$

Fig. 1(d) shows that material has clear $Nd_2Fe_{14}B$ phases with little CaO present as the CaO was removed from the fiber through the reaction with the NH_4Cl solution [16].

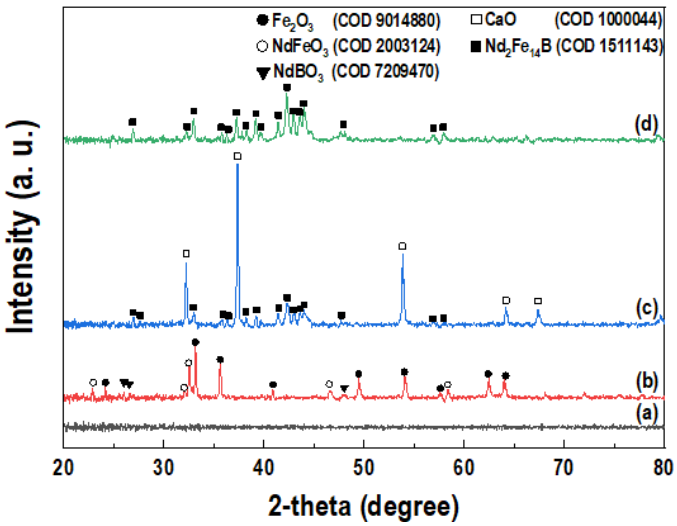

Fig. 1. X-ray diffraction patterns of Nd-Fe-B materials at each step: (a) as-spun, (b) calcination, (c) reduction, and (d) washing

Fig. 2 shows the SEM image of the synthesized Nd-Fe-B materials as a function of PVP concentrations at each heat treatment step. The viscosity of the precursor solution depends on the concentration of the PVP, which determines the thickness of the initial fiber. The viscosity values with increased PVP concentra-

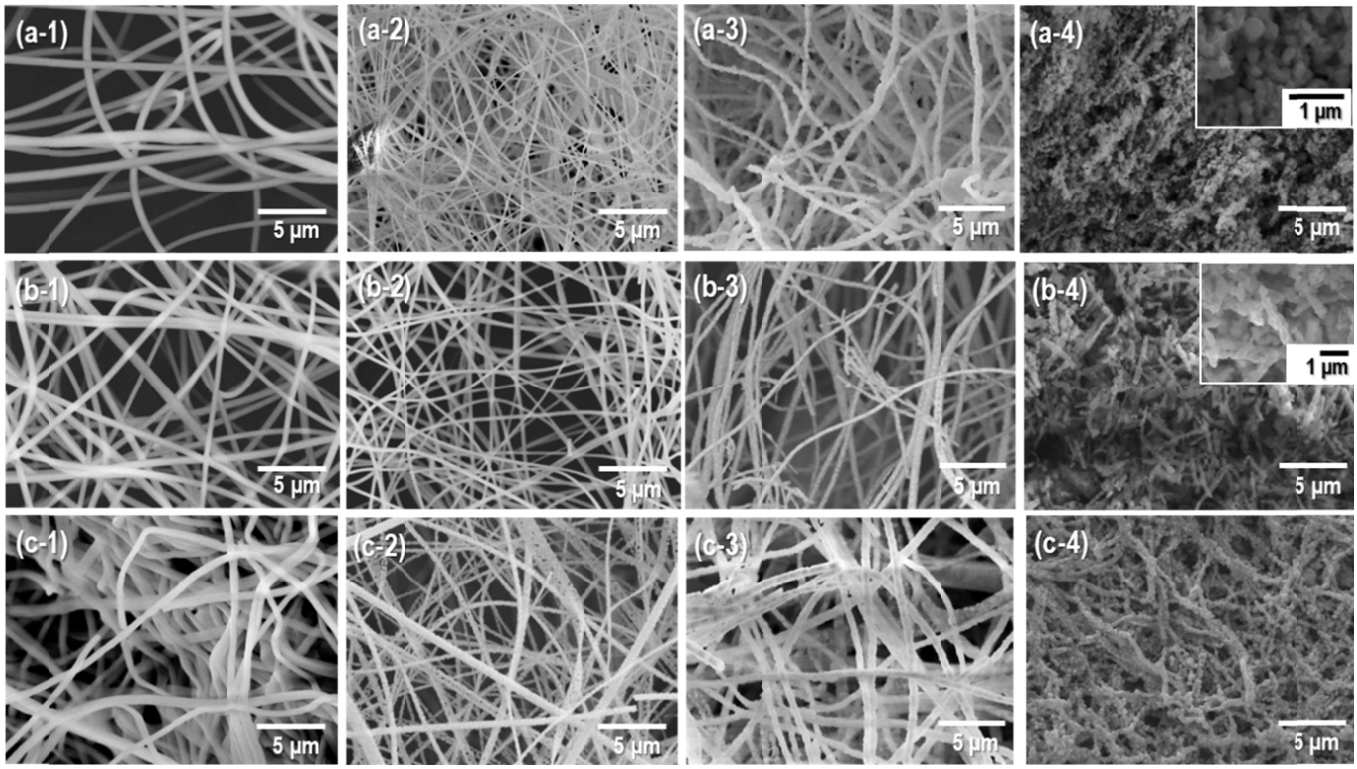

Fig. 2. SEM images of the synthesized Nd-Fe-B materials with different PVP concentrations at each step (as-spun, calcination, reduction, and washing): (a1-4) 3.15 wt%, (b1-4) 3.75 wt%, and (c1-4) 4.35 wt%

tion were estimated to be 76.8, 93.4 and 134.4 cP, respectively. In order to confirm the effect of the fiber thickness on the morphology, the thickness of the as-spun fiber and the oxide fiber were investigated. In the case of Fig. 2(a-1) and Fig. 2(a-2), the thickness decreased from 489 nm to 283 nm as as-spun fibers became oxide fibers; in Fig. 2(b-1) and Fig. 2(b-2), the thickness decreased from 541 nm to 334 nm; and in Fig. 2(c-1) and Fig. 2(c-2), the thickness decreased from 630 nm to 479 nm. As the PVP concentration decreased, the thickness of the fiber increased. It can be observed that the PVP concentration directly affects the thickness of the fiber before and after heat-treatment. Fig. 2(a) shows SEM images of the Nd-Fe-B materials in which the PVP concentration is 3.15 wt%, depicting continuous steps such as as-spun, calcination, reduction, and washing from Fig. 2(a-1) to Fig. 2(a-4). From Fig. 2(a-1) to (a-3), it can be seen that the material maintains the 1-dimensional morphology with a high aspect ratio. Fig. 2(a-4) shows the magnetic powders after washing with an NH_4Cl solution; it can be seen that during the washing process, the fibers were turned into powder. The morphology of Nd-Fe-B material with 3.75 wt% PVP concentration is shown in Fig. 2(b). The fiber morphology as in Fig. 2(a) can be observed before washing. However, Fig. 2(b-4) show that the fiber was turned into rods. Fig. 2(c) shows that Nd-Fe-B materials maintain the 1-dimensional fiber morphology throughout the process. The organic compounds were more or less removed from the fibers during heat-treatment, leading to surface pores [17] Oxide fiber becomes structurally unstable through shrinkage due to the reduction and alloying processes, which cause breakage in the washing process [18-20].

Fig. 3 shows the XRD patterns of $Nd_2Fe_{14}B$ materials after removal of CaO by washing. The XRD patterns revealed that only the $Nd_2Fe_{14}B$ phase was retained regardless of the morphology of the $Nd_2Fe_{14}B$ materials. There are no peaks of unreacted oxide and other materials like organics. The impurities, if exist, are below the XRD detection range.

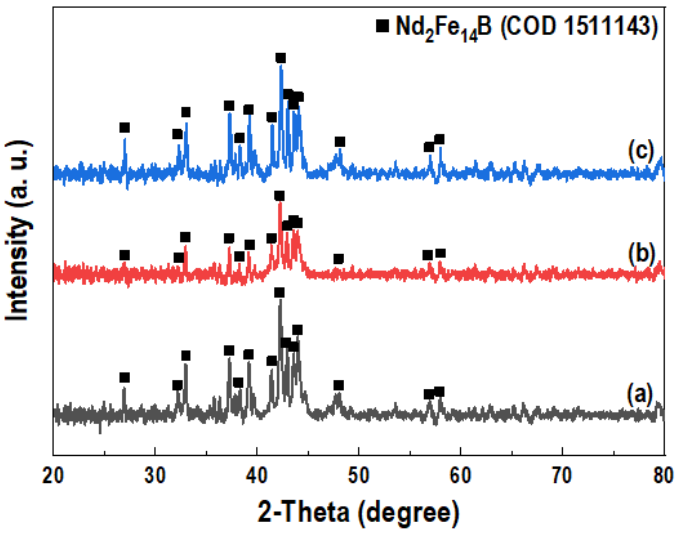

Fig. 3. X-ray diffraction patterns of $Nd_2Fe_{14}B$ materials synthesized with different PVP concentrations: (a) 3.15 wt% (b) 3.75 wt%, and (c) 4.35wt%

Fig. 4 is the VSM analyzed magnetic materials with different morphologies which were affected by the PVP concentration.

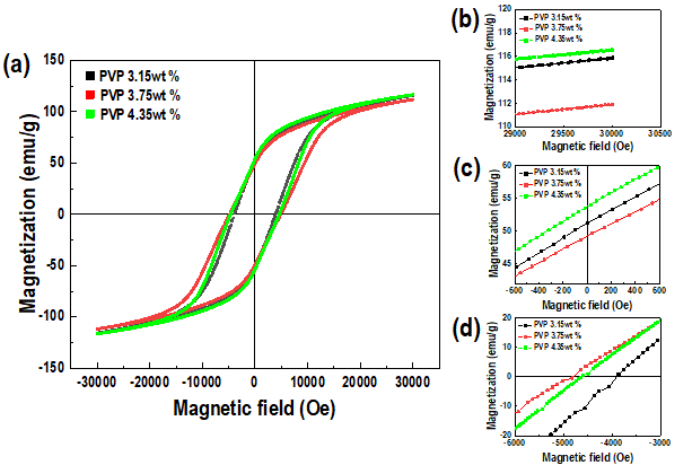

Fig. 4. Magnetic properties of the synthesized $Nd_2Fe_{14}B$ materials with different PVP concentrations: (a) M-H curve, (b) saturation magnetization (M_s), (c) remanence (M_r) and (d) coercivity (H_{ci})

These M-H hysteresis curves show three magnetic properties: saturation magnetization (M_s), remanence (M_r), and intrinsic coercivity (H_{ci}); the squareness (M_r/M_s) can also be calculated. In Fig. 4(a), it is seen that the ferromagnetic materials are not fully saturated. To fully saturate the material, the use of a 3-5 T magnetic field is required [19]. However, it should be possible to analyze the tendencies and characteristics of the magnetic materials produced through the results. There are slight differences in M_s and M_r between the powder and the fibers. Fig. 4(b) shows M_s close to 115 emu/g and Fig. 4(c) shows M_r close to 50 emu/g. The squareness (M_r/M_s) was about 0.44, which is the same for all samples. Through Fig. 4(d), the occurrence of some differences can be confirmed. As the PVP concentration was increased, the H_{ci} of the magnetic materials increased. The increase in H_{ci} is associated with the 1-dimensional morphology of the magnetic material affected by the shape anisotropy [6]; the powder had an H_{ci} of 3908 Oe, while the 1-dimensional rod has an H_{ci} of 4800 Oe. On the other hand, H_{ci} decreased to 4622 Oe when high aspect ratio 1-dimensional fibers were obtained. The particle size of the fiber became larger than the rod, and the H_{ci} value decreased because of the influence of the multi-domain structure [21].

4. Conclusions

Different morphologies such powders, rods and fibers in $Nd_2Fe_{14}B$ magnets were achieved by varying the concentration of PVP in the electrospinning process. All these materials had prominent $Nd_2Fe_{14}B$ phases, regardless of morphology. The VSM analysis showed that the coercivity increased by approximately 20% as it changed from the 0-dimension powder to the 1-dimension fiber morphology. These magnetic materials with 1-dimension morphology can have shape anisotropy due to their morphology. Using this fabrication method of the ternary magnet, we can adjust the morphology at the submicron scale from 0-dimensional to 1-dimensional, leading to a variety of properties.

Acknowledgments

This study has been performed with the support of Korea Institute of Industrial Technology titled “Development of one-dimensional FeNdB exchange coupling magnets manufacturing technology (UR190005)”.

REFERENCES

[1] C. Elinor, R. Sheridan, S. Grasso, A. Walton, M. Reece, J. Magn. Magn. Mater. **417**, 279-283 (2016).

[2] O. Gutfleisch, J. Appl. Phys. **33** (17), 157 (2000).

[3] T. Masaaki, S. Ikeda, Y. Morimoto, H. Kabashima, AIP Advances **6** (5) 056021 (2016).

[4] S. Hirosawa, Y. Matsuura, H. Yamamoto, S. Fujimura, M. Sagawa, H. Yamauchi, J. Appl. Phys. **59** (3), 873-879 (1986).

[5] X. Du, T.E. Graedel, J. Ind. Ecol. **15** (6), 836-843 (2011).

[6] K. Watanabe, B. Jinnai, S. Fukami, H. Sato, H. Ohno, Nat. Commun. **9** (1) 1-6 (2018).

[7] B.D. Cullity, C.D. Graham, Introduction to magnetic materials. 2nd ed., John Wiley & Sons. (2011).

[8] M. Sagawa, S. Fujimura, N. Togawa, H. Yamamoto, Y. Matsuura, J. Appl. Phys. **55** (6), 2083-2087 (1984).

[9] J.J. Croat, J.F. Herbst, R.W. Lee, F.E. Pinkerton, J. Appl. Phys. **55** (6), 2078-2082 (1984).

[10] Z.M. Huang, Y.-Z. Zhang, M. Kotaki, S. Ramakrishna, Compos. Sci. Technol. **63**, 2223-2253 (2003).

[11] A. Baji, Y.-W. Mai, S.-C. Wong, M. Abtahi, P. Chen, Compos. Sci. Technol. **70** (5), 703-718 (2010).

[12] N.S.A. Eom, S. Noh, M.A. Haq, B.S. Kim, J. Kor. Powder. Metall. Inst. **26** (6) 477-480 (2019).

[13] M. Fu, X. Li, R. Jiang, Z. Zhang, Appl. Surf. Sci. **441**, 239-250 (2018).

[14] X. Yin, M. Liu, B. Wan, Y. Zhang, W. Liu, Y. Wu, M. Yue, J. Rare Earths. **36** (1), 1284-1291 (2018).

[15] P.K. Deheri, V. Swaminathan, S.D. Bhame, Z. Liu, R.V. Ramanujan, Chem. Mater. **22** (24), 6509-6517 (2010)

[16] J. Lee, T.-Y. Hwang, H.-B. Cho, J. Kim, Y.-H. Choa, Sci. Rep. **8** (1), 1-11 (2018).

[17] E.J. Jeon, N.S.A. Eom, J. Lee, B. Lee, H.M. Cho, J.S. On, Y.-H. Choa, B.S. Kim, Arch. Metall. Mater. **63**, 1433 (2018).

[18] A.B. Fuertes, D. Alvarez, F. Rubiera, J.J. Pis, G. Marban, J.M. Palacos, Chem. Eng. Commun. **109** (1), 73-88 (1991).

[19] A.I. Persson, M.W. Larsson, S. Stenström, B.J. Ohlsson, L. Samuelson, L.R. Wallenberg, Nature Materials, **3** (10), 677-681 (2004).

[20] D. Brown, B.-M. Ma, Z. Chen, J. Magn. Magn. Mater. **248** (3), 432-440 (2002).

[21] P. Nothnagel, K.-H. Müller, D. Eckert, A. Handstein, J. Magn. Magn. Mater. **101** (1-3), 379-381 (1991).